Superior Valley Polarization and Coherence of 2s Excitons in Monolayer WSe_{2}

Shao-Yu Chen, Thomas Goldstein, Jiayue Tong, Takashi Taniguchi, Kenji Watanabe, and Jun Yan

Superior valley polarization and coherence of 2*s*

excitons in monolayer WSe$_2$

Shao-Yu Chen,[1] Thomas Goldstein,[1] Jiayue Tong,[1] Takashi Taniguchi,[2] Kenji Watanabe[2]

and Jun Yan[1,]*

[1]Department of Physics, University of Massachusetts, Amherst, Massachusetts 01003,

USA

[2]National Institute of Materials Science, 1-1 Namiki, Tsukuba, Ibaraki 305-0044, Japan

[*]Corresponding Author: Jun Yan.   Tel: (413)545-0853   Fax: (413)545-1691

E-mail: yan@physics.umass.edu

Abstract

We report experimental observation of 2*s* exciton radiative emission from monolayer tungsten diselenide, enabled by hexagonal boron nitride protected high-quality samples. The 2*s* luminescence is highly robust and persists up to 150K, offering a new quantum entity for manipulating the valley degree of freedom. Remarkably, the 2*s* exciton displays superior valley polarization and coherence than 1*s* under similar experimental conditions. This observation provides evidence that the Coulomb-exchange-interaction-driven valley-depolarization process, the Maialle-Silva-Sham mechanism, plays an important role in valley excitons of monolayer transition metal dichalcogenides.

The coupled spin-valley physics [1] in monolayer (1L) transition metal dichalcogenide (TMDC) semiconductors has inspired great strides towards realizing valleytronic devices harnessing these two-dimensional (2D) materials [2–5]. The two energetically degenerate 1L-TMDC valleys with opposite angular momentum can be selectively populated with circularly polarized optical excitation, and the valley polarization can be detected both optically [2–4] and electrically [5]. Further, coherent superposition of valley excitons can be generated with linearly polarized light [6] or a sequence of laser pulses with opposite circular polarization [7], which allows for rotation of the valley pseudospin with magnetic Zeeman effect or optical Stark effect [8,9]. Such coherent manipulations of valley pseudospin are at the heart of future quantum valleytronic devices, and require thorough understanding and efficient control of various valley depolarization and decoherence processes.

In general, intervalley scattering can occur due to both extrinsic mechanisms such as disorder scattering, and intrinsic mechanisms such as the Coulomb exchange interaction [10]; the competition between these different valley relaxation channels is a topic under active debate [7,11–13]. So far many of the valleytronic studies focus on the $1s$ exciton, the ground state of Coulomb-bound electron-hole pairs, which is readily accessible in 2D TMDC monolayers [2–9,14]. Excitons also have higher energy states that form the hierarchical Rydberg-like series [15–17], similar to hydrogen atoms. It is desirable to access the valley pseudospin of these higher quantum number exciton states, which in previous studies have been employed to demonstrate the exceptionally large exciton binding energy [15–19] and to probe exciton internal quantum transitions [20]. Yet it is relatively challenging to generate radiative emission from these states, as can be understood from Kasha's rule [21]: photon emission quantum yield is appreciable only for the lowest energy excited state, which for the charge neutral exciton, is the $1s$ state. In this Letter, we report that with efficient removal of disorder and phonon scattering channels, the $2s$ exciton luminescence from monolayer tungsten diselenide (1L-WSe$_2$) becomes accessible for valleytronic investigations. This is similar to the breaking of Kasha's rule in high-quality GaAs quantum wells [22], where the $2s$ luminescence becomes observable at low temperatures. We found the 1L-WSe$_2$ $2s$ exciton luminescence to be robust up to 150K, providing a new quantum entity for facile

manipulation of valley pseudospins. In contrast to 1*s*, 2*s* exciton exhibits much higher degree of valley polarization and coherence. This observation could be facilitated in part by the fast population decay of 2*s*, and our analysis further points to the action of intervalley Coulomb exchange interaction in TMDC pseudospin propagation, known as the Maialle-Silva-Sham (MSS) mechanism [10], which has been more elusive for charge neutral excitons [11–13] than for trions [6,23,24]. Our studies provide key insights into the TMDC intervalley scattering processes which are essential for developing TMDC-based valleytronic devices.

The 1L-WSe$_2$ samples used in our experiments are mechanically exfoliated from chemical vapor transport grown bulk crystals and are sandwiched between hexagonal boron nitride (*h*BN) flakes using a dry transfer technique (See Supplementary [25]). Figure 1a shows the luminescence excited by 2.33 eV photons and the differential reflectance spectra at 20K. In the upper panel, the luminescence spectrum displays a series of sharp peaks with narrow linewidth. The peak at 1.724eV, denoted as X_{1s}^0, is the neutral 1*s* exciton. Two peaks around 1.69eV separated by ~7meV are attributed to the coupled intra- and inter-valley trions split by the exchange interaction [6]. In the lower panel, a sharp peak at 1.855eV with full width half maximum (FWHM) of 4.8meV appears and we attribute it to the charge neutral 2*s* exciton luminescence (X_{2s}^0). The differential reflectance exhibits two prominent dips that match well to the X_{1s}^0 and X_{2s}^0 in the luminescence spectra. The near zero luminescence Stokes shift from the absorption dips [39] and the fully resolved negative trion doublet reflect the good sample quality [6,23,24].

Figure 1b shows the temperature dependence of luminescence emission from the sample. Both X_{1s}^0 and X_{2s}^0 blue shift with narrower linewidths at lower temperatures. In the Supplementary [25], we have performed detailed fittings and found that the peak position and linewidth evolution of X_{1s}^0 and X_{2s}^0 can be described by the same formulations. The temperature dependent intensities for the two neutral excitons are plotted in Fig.1c. The X_{1s}^0 intensity first increases and then decreases, peaking at about 150K. We note that this is distinct from previous WSe$_2$ samples that display monotonic 1*s* intensity decrease with lowering temperature [40], as a result of disorder scattering that depletes bright excitons into thermal equilibrium with lower energy dark excitons. The

excitons in 1L-WSe$_2$ are tightly bound [15] with large wavefunction overlap between the constituent electron and hole, giving rise to large exciton transition dipole oscillator strength and short radiative lifetime [20,41,42]. The non-monotonic 1s intensity temperature dependence is thus a manifestation of out-of-equilibrium exciton radiative recombination becoming more competitive with thermal equilibration between different quantum channels when disorder in the sample is minimized. In contrast, X_{2s}^0 does not show up until ~150K and its intensity keeps increasing with lowering temperature. Noting that the 2s-1s exciton energy separation is about 130meV, in the temperature range of our experiment, thermal distribution of the 2s exciton, unlike 1s, is largely negligible. The monotonic increase of 2s intensity at lower temperatures indicates that removal of phonon scattering enhances non-equilibrium 2s radiative emission, and further suggests that the 2s exciton also has a fast radiative recombination rate.

We note that there exists some controversy in the assignment of optical features with energies higher than the 1s exciton. Our observed 2s-1s separation of about 130meV is consistent with existing differential reflectance [15], photoluminescence excitation (PLE) measurements [43] and upconversion PL measurements [44], while a separate optical study inferred a much larger 2s-1s separation of 790meV [19]. Optical features in hBN sandwiched WSe$_2$ heterostructures are further complicated by inter-material exciton-phonon coupling that results in hybrid modes which do not appear in the optical spectra of either hBN or WSe$_2$ alone [45,46]. To confirm that the new emission feature we observe is from the 2s exciton, we performed two more control experiments. First, we fabricated an hBN-sandwiched field effect transistor device to tune this new peak by charge doping. We found that both X_{1s}^0 and X_{2s}^0 radiation become weaker and eventually disappear when the crystal is doped with electrons or holes (Supplementary [25] Fig.S3). This confirms that both X_{1s}^0 and X_{2s}^0 are associated with neutral excitons, consistent with our assignment. Second, we tuned the laser excitation across the X_{2s}^0 energy range to perform one photon PLE and resonant Raman scattering measurements. The X_{1s}^0 luminescence becomes more intense when the incident photon is in resonance with the X_{2s}^0 energy (Supplementary [25] Fig.S4). Further, two Raman bands R$_1$ and R$_2$ at 128 and 132meV become visible in Fig.2a, consistent with another recent Raman study that found a broad phonon feature in the range of 128-133meV (1030-1070cm^{-1}) [45]. These

5

two bands are assigned as the combinational modes [45,46] arising from the out-of-plane vibrations of WSe$_2$ (OC: out-of-plane chalcogen vibration [47], 31meV) and hBN (ZO: z-direction optical phonon; the infrared active 97meV A$_{2u}$ [48] and the optically silent 101meV B$_{1g}$ [49] phonons). The R$_1$ and R$_2$ bands have energies that are quite close to the 1s-2s energy separation; one possibility is that the X_{2s}^0 emission we observe are R$_1$ and R$_2$ phonon-exciton replicas of X_{1s}^0. We rule out that interpretation through two observations. One, as can be seen in Fig.2a, the combinational phonon bands are composed of two distinct peaks separated by ~4meV with a non-symmetric lineshape that depends sensitively on the resonance condition, while the X_{2s}^0 emission spectrum can be well-fitted by a Lorentzian function (Fig.1). Two, we measured the temperature dependence of the combinational phonon bands (Fig.2b) and found that the energy shift is opposite to that of the 1s-2s separation (Fig.2c and Supplementary [25] Fig.S5). This confirms that the X_{2s}^0 emission is not related to R$_1$ and R$_2$.

The appearance of the X_{2s}^0 emission in high-quality samples allows us to examine its valleytronic properties. Taking advantage of the valley dependent optical selection rule [1], we use circularly polarized light to selectively populate one valley and monitor the resultant valley polarization by examining the helicity of optical emission [2–4] . We also use linearly polarized light to create a coherent superposition of excitons in both K and K' valleys; the decoherence of the valley excitons are reflected in the degree of linear polarization of the luminescence emission [6]. Experimentally we excite our sample at 20K with σ_+ circularly polarized and H linearly polarized laser light that is detuned by 20meV above the exciton energy, and analyze the collected luminescence emission with σ_+, σ_-, H and V polarizations; see Fig.3a. The valley polarization and coherence are characterized by $P = \frac{I_{\sigma+\sigma+} - I_{\sigma+\sigma-}}{I_{\sigma+\sigma+} + I_{\sigma+\sigma-}}$ and $C = \frac{I_{HH} - I_{HV}}{I_{HH} + I_{HV}}$ respectively.

From Fig.3a, we found the 2s excitons to exhibit superior capability in retaining the broken time reversal symmetry and coherence of incident laser light with $P = 0.82$ and $C = 0.56$. Similar measurements are performed for the 1s exciton; see right panel of Fig.3a. Interestingly its $P = 0.15$ and $C = 0.17$ are significantly smaller than 2s, although the measurement was performed in the same sample at the same temperature with the laser energy also detuned at 20meV above the exciton energy.

The superior 2s valley polarization could be assisted by its fast population decay rate. As a higher energy state, the 2s exciton possesses decay channels such as the 2s-1s transition (See Supplementary [25]) not available to 1s. Indeed, X_{2s}^0 has a wider linewidth than X_{1s}^0 (4.8 vs. 4.0meV at 20K, see Fig.1a). If we assume the 0.8meV linewidth difference is mostly due to faster population decay, and take the 1s luminescence emission time to be 2ps from a recent study [50], we infer a 2s lifetime of about 0.6ps. Noting that the population decay time might be dependent on sample doping and substrate, we also estimated the ratio of the 1s and 2s lifetime using another approach: the 2s oscillator strength is about 15 times weaker than 1s from absorption spectra in Fig.1, consistent with the value from a recent diamagnetic shift measurement on a similar hBN sandwiched sample [51], while the low temperature 1s intensity is about 60 times stronger than 2s (Fig.1c). This suggests a decay rate ratio of 4, in reasonable agreement with the above estimation from linewidth difference. Assuming a phenomenological relation between P, the population and polarization decay time τ and τ_s: $P = \frac{1}{1+\tau/\tau_s}$, and using $P = 0.15$ and 0.82 for 1s and 2s, we find τ_s is about six times larger for 2s than for 1s. This indicates that the 2s exciton valley polarization is intrinsically more robust than 1s. Noting that the 2s and 1s excitons have the same symmetry, intervalley scattering allowed for 1s is thus anticipated to also affect the 2s valley pseudospins. Quantitatively however, the scattering rates may differ. In particular, the exchange interaction, capable of inducing intrinsic valley depolarization and decoherence through the MSS mechanism [10], differs substantially for 1s and 2s excitons. A recent study showed that MSS plays an important role in valley decoherence and observed a coherence time of about 100fs [7]. Below, we explain the drastically different valley polarization and coherence for 1s and 2s excitons in the framework of the exchange interaction MSS mechanism.

As illustrated in Fig.3b, the strong Coulomb interaction between the photo-generated electrons and holes not only gives rise to exceptionally large exciton binding energy [15], but also leads to the annihilation of bright excitons in one valley and creation in the other. This exchange of the excitons between the two valleys conserves energy but induces flipping of exciton angular momentum and pseudospin, compromising the valley

polarization and coherence. For excitons with center-of-mass momentum $\vec{k}$, the inter-valley exchange interaction is given by [52]

$$J_{\vec{k}} = -|\psi(r_{eh} = 0)|^2 \frac{a^2 t^2}{E_g^2} V(\vec{k}) k^2 e^{-2i\theta} \tag{1}$$

where $\psi(r_{eh})$ is the real space wavefunction for the relative motion between the electron and the hole, $a = 3.32\text{Å}$ is the lattice constant of monolayer WSe$_2$, t=1.19eV is the hopping energy, $E_g \approx$ 2eV is the band gap, $V(\vec{k})$ is the $\vec{k}$ component of the Coulomb interaction, and θ denotes the direction of $\vec{k}$. Effectively this exchange interaction introduces a pseudo-magnetic field acting on the valley pseudospin of the excitons. The angular dependence in Eqn.(1) implies that the direction of the pseudo-magnetic field depends on the direction of the exciton wavevector (Fig.3c). Consider, for example, a set of excitons with the same energy and pseudospin populated on a ring in the $\vec{k}$ space. The pseudo magnetic fields acting on them will have the same magnitude but different directions depending on the direction of $\vec{k}$. This makes the excitons on the ring to precess towards different directions, which in turn, causes valley depolarization and decoherence as the excitons propagate.

In Eqn.(1), $|\psi(r_{eh} = 0)|^2$ describes the probability density for the electron and the hole to spatially overlap. For the 1s exciton this is given approximately by $1/a_B^2$, where $a_B \approx$1.7nm [51] is the exciton Bohr radius. In the case of 2s excitons, a recent measurement found that the electron-hole separation in 2s is about 6.6nm [51]. Assuming that the 1s and 2s excitons have about the same mass, the 2s exchange interaction is then about 15 times weaker. This difference has an important impact on the exciton valley pseudospin dynamics. In Fig.3d, we simulated the pure exchange-interaction-driven valley depolarization and decoherence for excitons with different momentum k and kinetic energy $E_k = k^2/2M$: at $k = 0$, both P and C are equal to 1 since the exchange interaction in Eqn.(1) goes to zero at $k = 0$; for nonzero k, both P and C of 1s drops steeply at finite E_k, while for 2s the decrease is much slower, confirming that 1s is more impacted by the exchange depolarization fields.

It is of interest to note that for both 1s and 2s simulations in Fig.3d, C is always larger than P — this is a hallmark of exciton exchange interaction in 2D [10]: the exchange-interaction-induced pseudo-magnetic-fields are in the plane of the atomic layer,

8

thus the out-of-plane pseudospin of valley polarized excitons experiences the pseudo magnetic fields in two directions, while the in-plane pseudospin of the valley coherent excitons is relaxed only by the magnetic field component that is perpendicular to the pseudospin. Experimentally, we have observed C to be larger than P for $1s$ in Fig.3a as well as with many other laser excitations (more data in Supplementary [25] Fig.S4), further confirming that the exchange interaction dominates the $1s$ exciton valleytronic behavior. This is consistent with another recent study on high-quality MoS_2 where C is also found to be larger than P [53].

We note that for $2s$ excitons however, P is significantly larger than C as shown in Fig.3a. This suggests that with weaker $2s$ exchange interaction, other decoherence and depolarization mechanisms become more competitive. To account for these additional mechanisms, we have modified the model (see Supplementary [25]) such that even for k = 0, P and C are smaller than 1. This relatively simple model captures our observations semi-quantitatively: as shown in Fig.3e, for excitons with small kinetic energy (E_k < 1meV), P is mostly larger than C for $2s$ and smaller than C for $1s$, and numerically the $2s$ P and C values are much larger than $1s$.

We finally remark that the excitons can only become radiative if its momentum lies within the light cone, whose boundary corresponds to $1s$ and $2s$ exciton kinetic energy of ~10μeV. At such small E_k's the impact of exchange interaction is small. The large difference between P and C for $1s$ and $2s$ agrees with the conjecture that excitons outside the light cone with larger momentum provide a reservoir where disorder and phonon can scatter them into the light cone, which subsequently radiate [20]. The average exchange interaction that the radiatively recombined excitons experienced is thus much larger than the fields inside the light cone. In the supplementary [25], we show that it is possible to reduce the impact of exchange interaction fields on $1s$ by using the small-momentum $2s$ exciton as an alternative reservoir, corroborating another study of WSe_2 on SiO_2 [54]. Here with the presence of hBN, the $2s$ exciton can lose the excess ~130meV by emitting zero-momentum hBN-WSe_2 combinational phonons (Fig.2a). This reduces the number of phonons involved from six [54] to two, and markedly improves the $1s$ valley coherence and polarization to 0.64 and 0.30 respectively (Supplementary [25] Fig.S4).

In conclusion, we have accessed the 2s radiative emission in hBN sandwiched high-quality 1L-WSe$_2$ crystals. The 2s luminescence is highly robust and exhibits superior valleytronic properties. Our data provide evidence that the Maialle-Silva-Sham mechanism plays an importance role in the exciton valley decoherence and depolarization, which should be taken into account when developing valleytronic devices.

References:

[1] D. Xiao, G. Liu, W. Feng, X. Xu, and W. Yao, Phys. Rev. Lett. **108**, 196802 (2012).

[2] K. F. Mak, K. He, J. Shan, and T. F. Heinz, Nat. Nanotechnol. **7**, 494 (2012).

[3] H. Zeng, J. Dai, W. Yao, D. Xiao, and X. Cui, Nat. Nanotechnol. **7**, 490 (2012).

[4] T. Cao, G. Wang, W. Han, H. Ye, C. Zhu, J. Shi, Q. Niu, P. Tan, E. Wang, B. Liu, and J. Feng, Nat. Commun. **3**, 887 (2012).

[5] K. F. Mak, K. L. McGill, J. Park, and P. L. McEuen, Science **344**, 1489 (2014).

[6] A. M. Jones, H. Yu, N. J. Ghimire, S. Wu, G. Aivazian, J. S. Ross, B. Zhao, J. Yan, D. G. Mandrus, D. Xiao, W. Yao, and X. Xu, Nat. Nanotechnol. **8**, 634 (2013).

[7] K. Hao, G. Moody, F. Wu, C. K. Dass, L. Xu, C.-H. Chen, L. Sun, M.-Y. Li, L.-J. Li, A. H. MacDonald, and X. Li, Nat. Phys. **12**, 677 (2016).

[8] R. Schmidt, A. Arora, G. Plechinger, P. Nagler, A. Granados del Águila, M. V.

Ballottin, P. C. M. Christianen, S. Michaelis de Vasconcellos, C. Schüller, T. Korn, and R. Bratschitsch, Phys. Rev. Lett. **117**, 77402 (2016).

[9]   Z. Ye, D. Sun, and T. F. Heinz, Nat. Phys. **13**, 26 (2016).

[10]   M. Z. Maialle, E. A. de Andrada e Silva, and L. J. Sham, Phys. Rev. B **47**, 15776 (1993).

[11]   H. Dery and Y. Song, Phys. Rev. B **92**, 125431 (2015).

[12]   G. Kioseoglou, A. T. Hanbicki, M. Currie, A. L. Friedman, and B. T. Jonker, Sci. Rep. **6**, 25041 (2016).

[13]   G. Wang, E. Palleau, T. Amand, S. Tongay, X. Marie, and B. Urbaszek, Appl. Phys. Lett. **106**, 112101 (2015).

[14]   T. Yan, J. Ye, X. Qiao, P. Tan, and X. Zhang, Phys. Chem. Chem. Phys. **19**, 3176 (2017).

[15]   K. He, N. Kumar, L. Zhao, Z. Wang, K. F. Mak, H. Zhao, and J. Shan, Phys. Rev. Lett. **113**, 26803 (2014).

[16]   A. Chernikov, T. C. Berkelbach, H. M. Hill, A. Rigosi, Y. Li, O. B. Aslan, D. R. Reichman, M. S. Hybertsen, and T. F. Heinz, Phys. Rev. Lett. **113**, 76802 (2014).

[17]   H. M. Hill, A. F. Rigosi, C. Roquelet, A. Chernikov, T. C. Berkelbach, D. R. Reichman, M. S. Hybertsen, L. E. Brus, and T. F. Heinz, Nano Lett. **15**, 2992 (2015).

[18]   Z. Ye, T. Cao, K. O'Brien, H. Zhu, X. Yin, Y. Wang, S. G. Louie, and X. Zhang, Nature **513**, 214 (2014).

[19]   A. T. Hanbicki, M. Currie, G. Kioseoglou, A. L. Friedman, and B. T. Jonker, Solid State Commun. **203**, 16 (2015).

[20]   C. Poellmann, P. Steinleitner, U. Leierseder, P. Nagler, G. Plechinger, M. Porer, R. Bratschitsch, C. Schüller, T. Korn, and R. Huber, Nat. Mater. **14**, 889 (2015).

[21]   M. Kasha, Discuss. Faraday Soc. **9**, 14 (1950).

[22]   K. J. Moore, P. Dawson, and C. T. Foxon, Phys. Rev. B **34**, 6022 (1986).

[23]   A. M. Jones, H. Yu, J. R. Schaibley, J. Yan, D. G. Mandrus, T. Taniguchi, K. Watanabe, H. Dery, W. Yao, and X. Xu, Nat. Phys. **12**, 323 (2015).

[24]   A. Singh, K. Tran, M. Kolarczik, J. Seifert, Y. Wang, K. Hao, D. Pleskot, N. M. Gabor, S. Helmrich, N. Owschimikow, U. Woggon, and X. Li, Phys. Rev. Lett.

117, 257402 (2016).

[25] See Supplemental Material at [url], which includes Supplemental Refs. [26–38], for additional details on sample preparation, optical setup, supporting experiments and analysis, as well as valley depolarization and decoherence model.

[26] L. Wang, I. Meric, P. Y. Huang, Q. Gao, Y. Gao, H. Tran, T. Taniguchi, K. Watanabe, L. M. Campos, D. A. Muller, J. Guo, P. Kim, J. Hone, K. L. Shepard, and C. R. Dean, Science **342**, 614 (2013).

[27] S.-Y. Chen, T. Goldstein, D. Venkataraman, A. Ramasubramaniam, and J. Yan, Nano Lett. **16**, 5852 (2016).

[28] S.-Y. Chen, C. H. Naylor, T. Goldstein, A. T. C. Johnson, and J. Yan, ACS Nano **11**, 814 (2017).

[29] T. Goldstein, S.-Y. Chen, J. Tong, D. Xiao, A. Ramasubramaniam, and J. Yan, Sci. Rep. **6**, 28024 (2016).

[30] K. P. O'Donnell and X. Chen, Appl. Phys. Lett. **58**, 2924 (1991).

[31] M. Selig, G. Berghäuser, A. Raja, P. Nagler, C. Schüller, T. F. Heinz, T. Korn, A. Chernikov, E. Malic, and A. Knorr, Nat. Commun. **7**, 13279 (2016).

[32] H. Sahin, S. Tongay, S. Horzum, W. Fan, J. Zhou, J. Li, J. Wu, and F. M. Peeters, Phys. Rev. B **87**, 165409 (2013).

[33] G. Moody, C. Kavir Dass, K. Hao, C.-H. Chen, L.-J. Li, A. Singh, K. Tran, G. Clark, X. Xu, G. Berghäuser, E. Malic, A. Knorr, and X. Li, Nat. Commun. **6**, 8315 (2015).

[34] B. Fallahazad, H. C. P. Movva, K. Kim, S. Larentis, T. Taniguchi, K. Watanabe, S. K. Banerjee, and E. Tutuc, Phys. Rev. Lett. **116**, 86601 (2016).

[35] G.-B. Liu, W.-Y. Shan, Y. Yao, W. Yao, and D. Xiao, Phys. Rev. B **88**, 85433 (2013).

[36] S. Fang, R. Kuate Defo, S. N. Shirodkar, S. Lieu, G. A. Tritsaris, and E. Kaxiras, Phys. Rev. B **92**, 205108 (2015).

[37] T. C. Berkelbach, M. S. Hybertsen, and D. R. Reichman, Phys. Rev. B **88**, 45318 (2013).

[38] D. Y. Qiu, F. H. da Jornada, and S. G. Louie, Phys. Rev. Lett. **111**, 216805 (2013).

[39] F. Yang, M. Wilkinson, E. J. Austin, and K. P. O'Donnell, Phys. Rev. Lett. **70**, 323

(1993).

[40] X.-X. Zhang, Y. You, S. Y. F. Zhao, and T. F. Heinz, Phys. Rev. Lett. **115**, 257403 (2015).

[41] M. Palummo, M. Bernardi, and J. C. Grossman, Nano Lett. **15**, 2794 (2015).

[42] H. Wang, C. Zhang, W. Chan, C. Manolatou, S. Tiwari, and F. Rana, Phys. Rev. B **93**, 45407 (2016).

[43] G. Wang, X. Marie, I. Gerber, T. Amand, D. Lagarde, L. Bouet, M. Vidal, A. Balocchi, and B. Urbaszek, Phys. Rev. Lett. **114**, 97403 (2015).

[44] M. Manca, M. M. Glazov, C. Robert, F. Cadiz, T. Taniguchi, K. Watanabe, E. Courtade, T. Amand, P. Renucci, X. Marie, G. Wang, and B. Urbaszek, Nat. Commun. **8**, 14927 (2017).

[45] C. Jin, J. Kim, J. Suh, Z. Shi, B. Chen, X. Fan, M. Kam, K. Watanabe, T. Taniguchi, S. Tongay, A. Zettl, J. Wu, and F. Wang, Nat. Phys. **13**, 127 (2016).

[46] C. M. Chow, H. Yu, A. M. Jones, J. Yan, D. G. Mandrus, T. Taniguchi, K. Watanabe, W. Yao, and X. Xu, Nano Lett. **17**, 1194 (2017).

[47] S.-Y. Chen, C. Zheng, M. S. Fuhrer, and J. Yan, Nano Lett. **15**, 2526 (2015).

[48] R. Geick, C. H. Perry, and G. Rupprecht, Phys. Rev. **146**, 543 (1966).

[49] J. Serrano, A. Bosak, R. Arenal, M. Krisch, K. Watanabe, T. Taniguchi, H. Kanda, A. Rubio, and L. Wirtz, Phys. Rev. Lett. **98**, 95503 (2007).

[50] C. Robert, D. Lagarde, F. Cadiz, G. Wang, B. Lassagne, T. Amand, A. Balocchi, P. Renucci, S. Tongay, B. Urbaszek, and X. Marie, Phys. Rev. B **93**, 205423 (2016).

[51] A. V. Stier, N. P. Wilson, K. A. Velizhanin, J. Kono, X. Xu, and S. A. Crooker, arXiv:1709.00123 (2017).

[52] H. Yu, G.-B. Liu, P. Gong, X. Xu, and W. Yao, Nat. Commun. **5**, 35 (2014).

[53] F. Cadiz, E. Courtade, C. Robert, G. Wang, Y. Shen, H. Cai, T. Taniguchi, K. Watanabe, H. Carrere, D. Lagarde, M. Manca, T. Amand, P. Renucci, S. Tongay, X. Marie, and B. Urbaszek, Phys. Rev. X **7**, 21026 (2017).

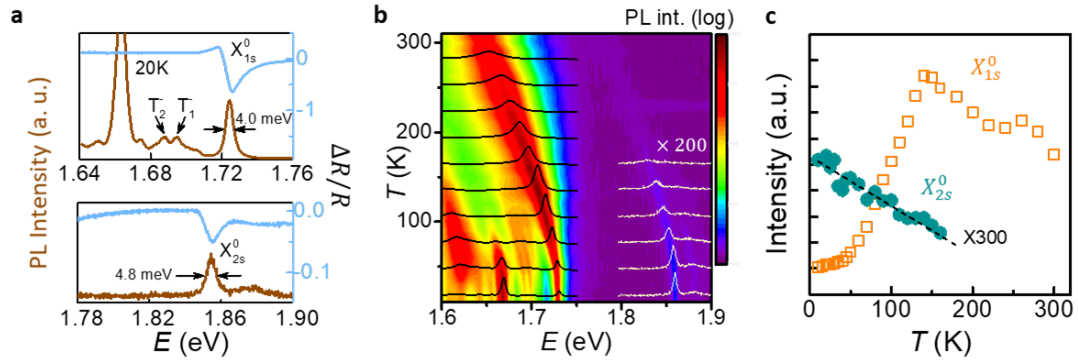[54] G. Wang, M. M. Glazov, C. Robert, T. Amand, X. Marie, and B. Urbaszek, Phys. Rev. Lett. **115**, 117401 (2015).

Figure 1 (**a**) The photoluminescence excited by 2.33eV laser light (brown) and the differential reflectance (light blue) spectra at 20K. The FWHM of 1s (X_{1s}^0) and 2s (X_{2s}^0) are 4.0 and 4.8meV, respectively. (**b**) Photoluminescence spectra plotted as a function of temperature. Selected spectra at $T = 10$ to 280K with 30K steps are displayed. (**c**) Temperature dependences of 1s and 2s intensity.
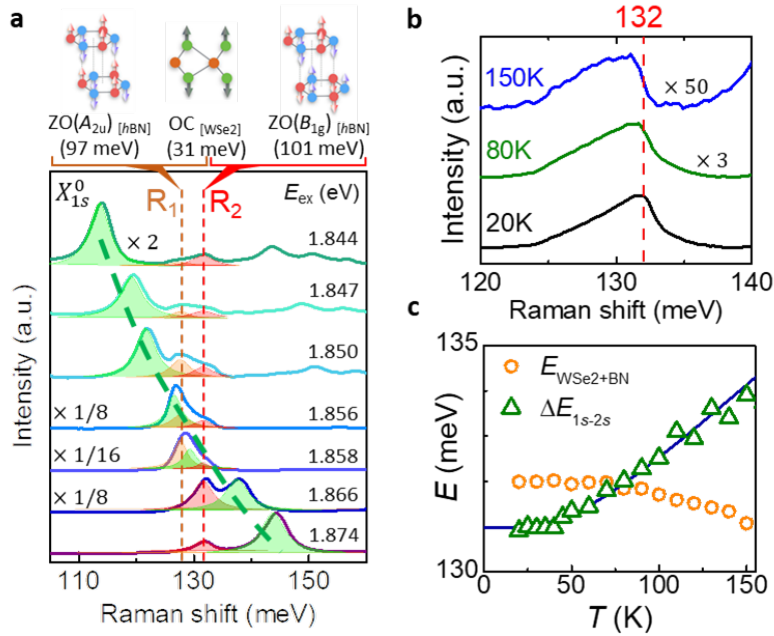
Figure 2 (**a**) Resonant Raman scattering of R_1 and R_2 using photon energies from 1.844 to 1.874eV. The peaks guided by the green dashed curve are the $1s$ exciton luminescence. (**b**) Raman scattering of the WSe_2/BN combinational modes at 20K, 80K and 150K. The dash line is aligned with 132meV. (**c**) The temperature dependence of $1s$ and $2s$ exciton energy separation (ΔE_{1s-2s}) and WSe_2/BN combinational phonon energy.
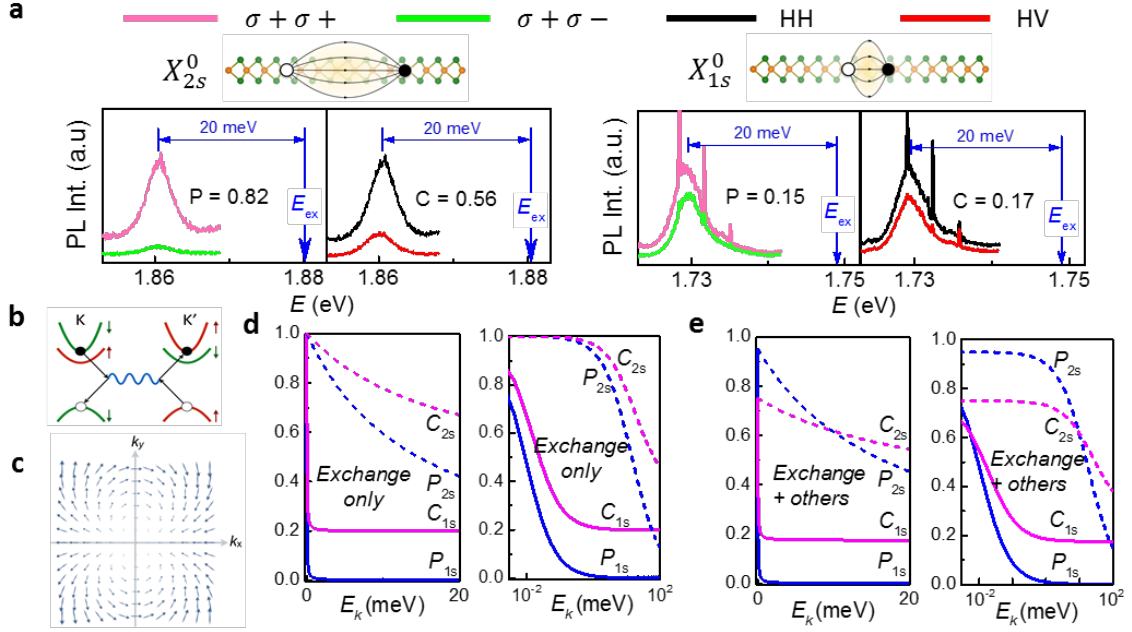
Figure 3 (a) The circular and linear polarization-resolved photoluminescence of 1L-WSe$_2$ at 20K with detuned excitation photon energy at 20meV above 2s (left) and 1s (right) excitons. **(b)** A schematic showing the inter-valley electron-hole exchange interaction, which induces pseudospin flip. **(c)** The strength and direction of the inter-valley exchange pseudo-magnetic field in k-space. **(d)** The simulated valley coherence (C) and polarization (P) as a function of E_k for 1s and 2s excitons considering pure exchange interactions. The left (right) panel is in linear (semilog) scale. **(e)** Simulated C and P considering both exchange interactions and other depolarization and decoherence mechanisms.